nature photonics

Article

https://doi.org/10.1038/s41566-023-01226-9

Unidirectional unpolarized luminescence emission via vortex excitation

Received: 10 June 2022

Accepted: 2 May 2023

Published online: 12 June 2023

Check for updates

Jincheng Ni[1,2,5], Shengyun Ji[2,3,5], Zhenyu Wang[2], Shunli Liu[2], Yanlei Hu[2], Yang Chen[2], Jiawen Li[2], Xiangping Li[4], Jiaru Chu[2], Dong Wu[2] ✉ & Cheng-Wei Qiu[1] ✉

Controlling the direction of light emission on the subwavelength scale is a key capability for quantum information processing and optical imaging in photonics and biology[1–5]. The spin–orbit interaction of light is widely adopted for dynamically tuning the direction of circularly polarized photoluminescence (PL), but this is challenging to accomplish for many luminescence materials, which typically generate unpolarized luminescence. Here, we report optical control of unidirectional emission of unpolarized luminescence in a spatially symmetric nanopillar lattice assisted by photonic orbital angular momenta. The orientation of anti-Stokes shift PL emissions can be controlled by the helicity of incident vortex beams. The experimental directionality of unpolarized PL emission in the one-dimensional nanopillar lattice can reach 0.59, which is markedly stronger than that possible by a spin mechanism. Our findings thus offer a new promising approach for tuneable nanoscale optical control of emission.

Control over the directional propagation properties of nanoscale luminescence emitters is key to manipulating light and improving efficiency in optical sensing and quantum information processing[1,2]. Emission of photoluminescence (PL), which is incoherent and unpolarized in free space, typically involves large solid angles because their interaction with excited light is omnidirectional. A combination of the quantum luminescence emitters and nanophotonic cavities makes it possible to tailor the spatiotemporal properties of PL. Recently, it was reported that the direction and polarization states of emitted luminescence can be controlled by integration with suitable nanostructures such as optical antenna arrays[3], silicon nanowires[4], metasurfaces[5] and photonic crystals[6]. In particular, the directional emission can be achieved through phasing between different nanoscale elements such as Yagi–Uda antenna arrays[3] and phase-gradient metasurfaces[5]. Although the phase-gradient metasurfaces have demonstrated some degree of control over spontaneous emission, the direction of luminescence emission is typically non-adjustable for such spatially asymmetric nanostructures.

Photonic angular momenta may serve as an effective solution for flexibly switching the directionality of PL emission. For example, the spin–orbit interaction of light has been employed to tune the directional propagation of surface-plasmon polaritons[7–10], where incident circularly polarized light provides spin angular momentum (SAM). Such spin-directional propagation in spatially symmetric nanostructures has stimulated the development of chiral quantum optics[1,11,12]. More recently, the valley pseudospin of two-dimensional transition metal dichalcogenide materials was reported to enable the directional emission of luminescence[13–16], which possesses valley-dependent circularly polarized states (Fig. 1a). However, such directional emission controlled by spin–orbit coupling is challenging for most luminescence emitters because the excited PL typically demonstrates unpolarized states from spontaneous emission[17]. As shown in Fig. 1b, the unpolarized PL, where two spin components have equal probability, results in symmetric emission in the spatially symmetric nanostructures[18].

[1]Department of Electrical and Computer Engineering, National University of Singapore, Singapore, Singapore. [2]Chinese Academy of Sciences Key Laboratory of Mechanical Behavior and Design of Materials, Department of Precision Machinery and Precision Instrumentation, University of Science and Technology of China, Hefei, China. [3]Department of Biomedical Engineering, Washington University in St. Louis, St. Louis, MO, USA. [4]Guangdong Provincial Key Laboratory of Optical Fiber Sensing and Communications, Institute of Photonics Technology, Jinan University, Guangzhou, China. [5]These authors contributed equally: Jincheng Ni, Shengyun Ji. ✉e-mail: dongwu@ustc.edu.cn; chengwei.qiu@nus.edu.sg

https://doi.org/10.1038/s41566-023-01226-9

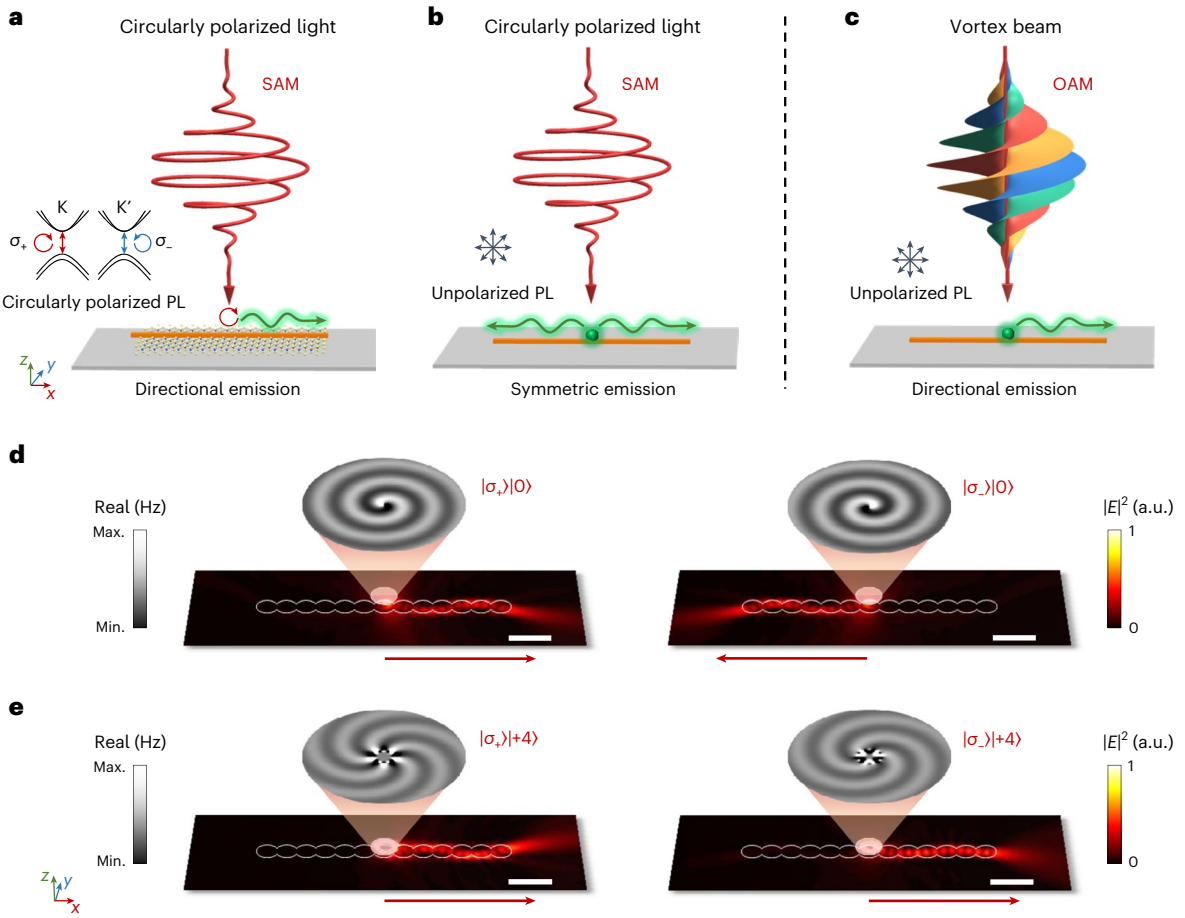

Fig. 1 | Concept of directional emission of unpolarized luminescence by vortex beams. a, Illustration of the directional emission of luminescence by spin–orbit coupling in a nanoscale waveguide. The circularly polarized luminescence can be generated by valley-dependent excitation on two-dimensional transition metal dichalcogenide materials. **b**, The symmetric emission of unpolarized luminescence excited by circularly polarized light. The spin information of incident light is lost in the excited luminescence. **c**, Schematic of directional emission of unpolarized luminescence excited by vortex beams. **d**, Simulation of unidirectional propagation of an electromagnetic wave in the one-dimensional nanopillar lattice excited by σ_+ (left panel) and σ_- (right panel) circular dipoles, respectively. **e**, Unidirectional propagation excited by σ_+ (left panel) and σ_- (right panel) vortex sources with topological charge $\ell = +4$. Red arrows indicate the preferred propagation direction. Scale bars, 1 μm (**d**,**e**).

Unlike the SAM with only two states of $\pm\hbar$ (where $\hbar$ is the reduced Planck's constant), the intrinsic orbital angular momentum (OAM) has unlimited orthogonal eigenstates in principle and has been realized in different wave fields such as electron[19], sound[20] and even molecular waves[21]. Vortex beams, carrying photonic OAM of $\ell\hbar$ with a phase singularity in the optical field centre, have an azimuthal phase distribution of $\sim e^{i\ell\varphi}$, where integer ℓ is topological charge and φ is the azimuthal angle[22,23]. The photonic OAM has been considered as a promising solution to boost the capacity of data transmission and storage in next-generation optical communications and quantum information processing[24–28]. Recently, it was reported that OAM beams can selectively excite PL in nanowires by sophisticated plasmonic nanogrooves[29]. Analogous to the spin–orbit interaction of light, the orbit–orbit interaction has been exploited in some theoretical and experimental studies[7,30,31], but the orbit-directional PL emission remains elusive mainly due to the lack of phase-locking luminescence. Here, we experimentally demonstrate the unidirectional emission of unpolarized PL in spatially symmetric nanostructures by photonic OAM at room temperature (Fig. 1c). Distinguished from polarization-dependent directionality, the unpolarized PL emission is controlled by the OAM states of vortex beams, which are linked to the helical phase information.

To confirm the predictions of directional propagation, we performed the full-wave finite-difference time-domain simulations excited by electric dipoles (Methods). The left- and right-handed circularly polarized dipoles $\sigma_+ = (\hat{x} \pm i\hat{y})/\sqrt{2}$ excite opposite chiral electromagnetic fields, which can directionally couple into a one-dimensional nanopillar lattice by spin–orbit coupling[10] (Fig. 1d). The intensity distributions in the nanopillar lattice are mirror-symmetric for $\sigma_\pm$ circular dipoles. Therefore, the unpolarized luminescence, which has the same possibility for generating $\sigma_\pm$ circular dipoles, results in symmetric emission. When introducing a high-order topological charge $\ell = +4$, the chiral electromagnetic fields excited by $\sigma_\pm$ vortex sources break the spatially symmetric properties, as shown in Fig. 1e. We can define the topological charge of the chiral H_z fields excited by the vortex source as:

$$j_z = \frac{1}{2\pi}\oint_C \mathrm{d}\boldsymbol{r}\nabla_{\boldsymbol{r}}\phi(\boldsymbol{r})$$

where C is a closed loop around the phase singularity, $\boldsymbol{r}$ is the radial distance and ϕ is the phase distribution. Owing to the conservation of the angular momentum of the z-component, the total intrinsic angular momentum of the excited chiral field is determined by $j_z = \ell + \sigma$, where $\sigma = \pm 1$ per photon[32–34] (see Supplementary Note 1 for details). Distinguished from the only spin scenarios, the electromagnetic wave excited by a vortex source with $\ell = +4$ shows an identical propagating direction

https://doi.org/10.1038/s41566-023-01226-9

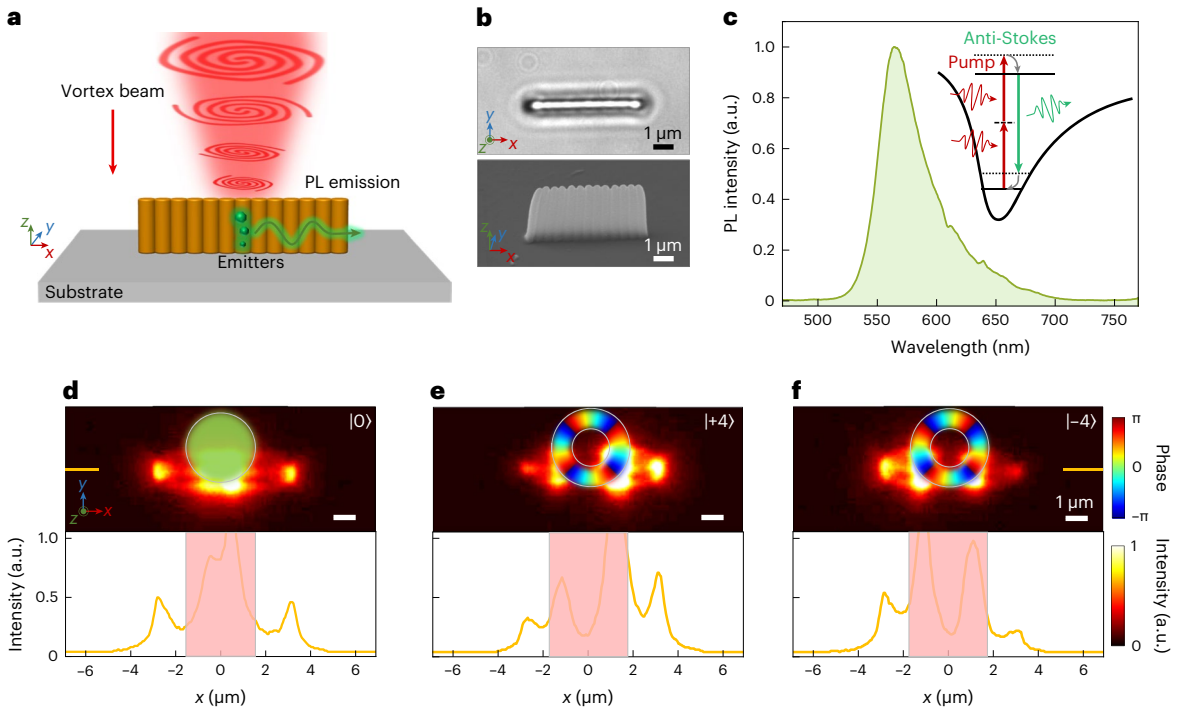

Fig. 2 | Experimental measurements of unidirectional propagation in the nanopillar lattice. a, Schematic of the nanopillar system under focused vortex beams showing the possible excitation of electric-dipole resonances. Unpolarized PL emitters are generated in the central nanopillars by two-photon absorption for orbit-directional coupling. **b**, Optical (top panel) and SEM images (bottom panel) of the fabricated one-dimensional nanopillar lattice. The nanopillar lattice consists of 13 nanopillars with height $h = 3.8$ μm, diameter $d = 500$ nm and period $p = 440$ nm. **c**, Anti-Stokes shift PL spectrum of the nanopillar system excited by a vortex beam at the fundamental wavelength of 800 nm. **d**–**f**, The luminescence image (top panel) and line cut of the intensity profiles (bottom panel) along the nanopillar system excited by the vortex beam with topological charge $\ell = 0$ (**d**), +4 (**e**) and −4 (**f**), respectively.

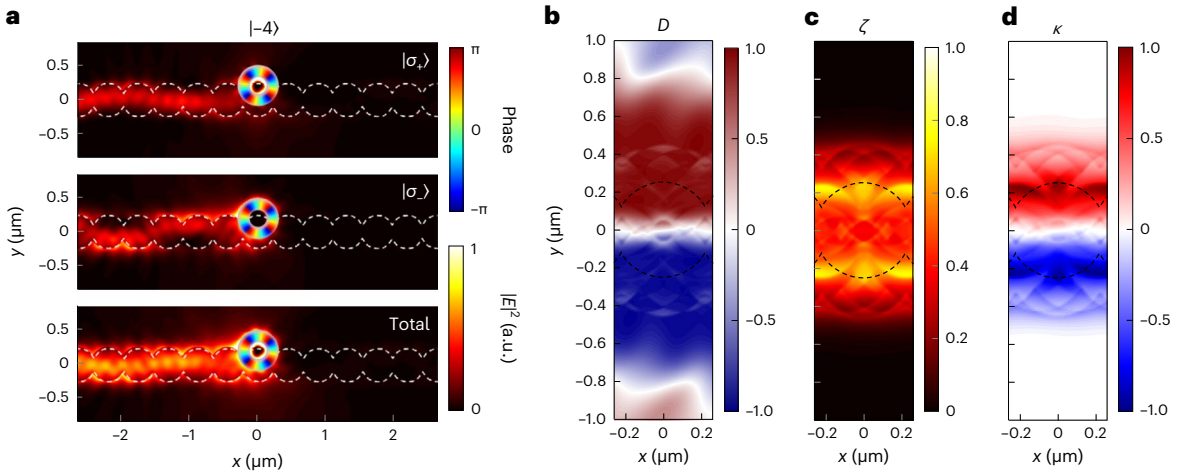

Fig. 3 | Numerical simulations of unidirectional propagation by vortex sources. a, Electric-field intensity distribution in the nanopillar system excited by σ_+ (top panel) and σ_- (middle panel) vortex sources with topological charge $\ell = -4$. The bottom panel shows the total intensity distribution, where two spin components exist equally. **b**, Directionality D for the radiation of vortex source with topological charge $\ell = -4$ as a function of its excited position. **c**, Normalized coupling strength ζ of the vortex source into the nanopillar lattice. **d**, The directional coupling efficiency, which indicates the directionality modulated by coupling efficiency $\kappa_{(x,y)} = D_{(x,y)} \times \zeta_{(x,y)}$, for the vortex source radiation. Dashed lines indicate the position of the nanopillar system.

for both $\sigma = \pm 1$ after coupling into the nanopillar lattice. As a result, for the unpolarized luminescence with a total zero SAM ($\sigma = 0$), we may still realize the unidirectional emission by introducing a high-order topological charge for a non-zero j_z state.

Our experimental configuration for the unidirectional luminescence emission consisted of incident vortex beams with tunable topological charges and a one-dimensional nanopillar lattice, as shown in Fig. 2a. The nanopillar lattice was fabricated by a direct-laser-writing method in a polymer material, which contained luminescence molecules (Methods). Figure 2b shows the optical and scanning electron microscope (SEM) images of the fabricated nanopillar lattice. Distinguished from the gradient phase from metasurfaces with spatially asymmetric nanostructures[3,5], the helical phase information in our experiments was achieved from the incident vortex beams (Supplementary Note 2). We used a home-built optical microscope system with a femtosecond laser excitation at the central wavelength of 800 nm

https://doi.org/10.1038/s41566-023-01226-9

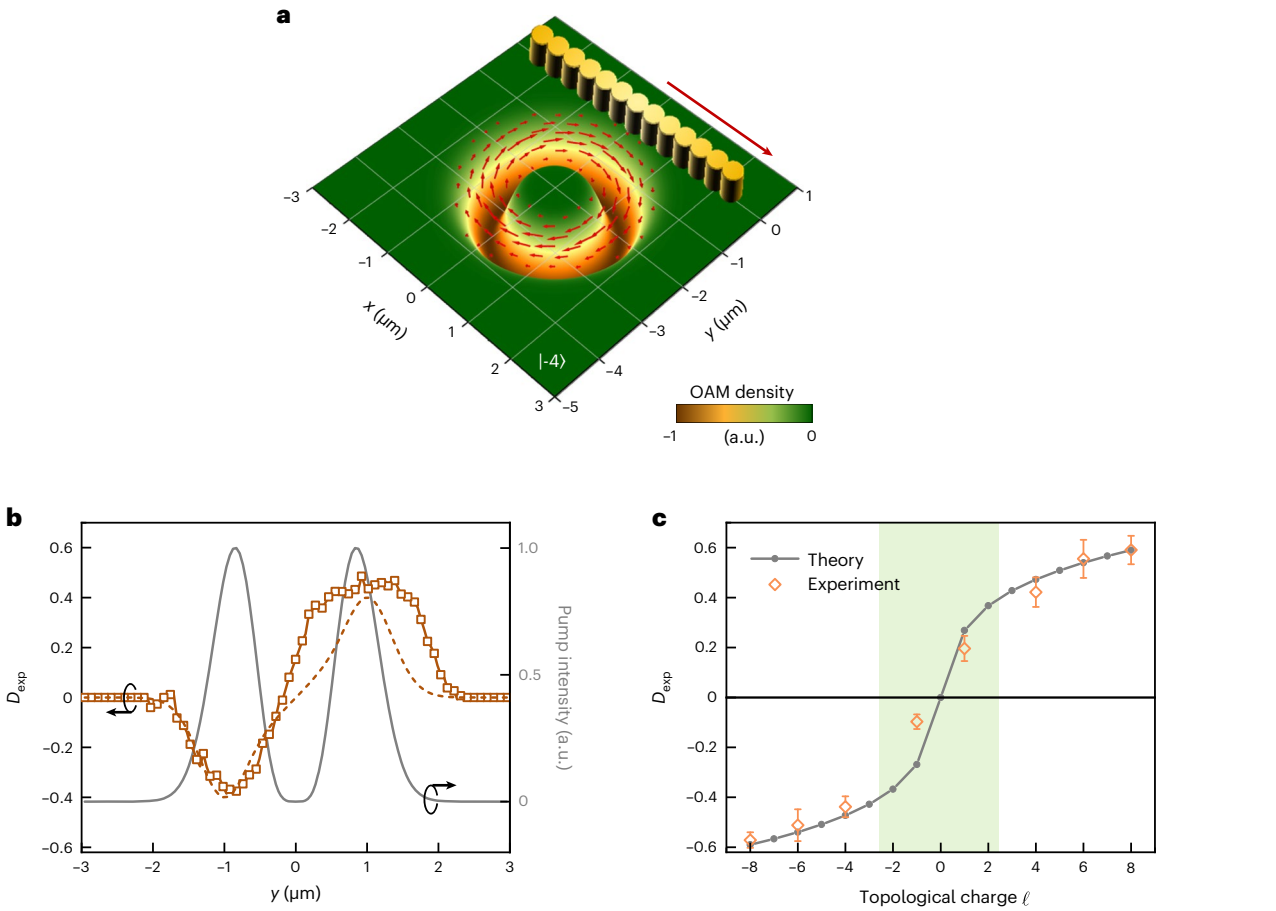

Fig. 4 | OAM-dependent PL unidirectional emission. a, Simulated OAM density of the vortex beam with topological charge $\ell = -4$ on the transverse plane. The red arrows indicate the in-plane momentum density. The one-dimensional nanopillar lattice (not to scale) is excited by the vortex beam at different y positions. **b**, Experimental (solid line) and theoretical (dashed line) directionality of PL emission as a function of the nanopillar position excited by the vortex beam with topological charge $\ell = -4$. The grey line indicates the pump intensity distribution of the incident vortex beam. **c**, Extreme directionality of PL emission for vortex beams with varying topological charges. The green region indicates the excitation by vortex beams with topological charge $\ell = \pm 1$. The error bars are the standard deviation of five measurements. All excited positions are located in the $y < 0$ region.

(Supplementary Fig. 10). When the femtosecond laser was focused into the luminescence material, the focused region produced high-energy photons by two-photon absorption, converting the near-infrared radiation into visible luminescence (Supplementary Fig. 11). The PL spectrum was collected from the nanopillar lattice, excited by a vortex beam at the laser power of 40 mW (Fig. 2c). The central wavelength of anti-Stokes shift PL emission was at ~560 nm.

In our experiments, the anti-Stokes shift PL can be excited only at the focused area of a vortex beam, where enough photon density can be provided for two-photon absorption. An optical short-pass filter was used in our experiments to block the fundamental frequency light, for collecting the PL emission images only. Raw data are presented in Fig. 2d–f for vortex beams with different topological charges of $\ell = 0$, +4 and −4. The centre of the excited vortex beams is located at a fixed displacement of $y = 1$ μm away from the nanopillar lattices. For the topological charge of $\ell = 0$, PL intensity at the left-hand and right-hand ends of the nanopillar system are nearly equal, which implies symmetric emission (Fig. 2d). The large central spot is caused by anti-Stokes shift PL scattering in the focused area. PL intensity at both ends of the nanopillar system is obviously lower due to the small transverse momentum in excited luminescence. Excited by the vortex beam with $\ell = +4$, we observed a clear directional propagation to the right-hand end of the nanopillar system (Fig. 2e). When the helicity of the vortex beam flips, the propagating direction of the PL emission is changed to another end, as shown in Fig. 2f. The focal sizes of the vortex beam are ~2 μm for topological charges $\ell = \pm 4$ (Supplementary Fig. 12). The PL intensity scattered at the left-hand and right-hand ends of the nanopillar system can be used to quantify the unidirectional PL emission. We define the experimental directionality of PL emission as $D_{exp} = (I_L - I_R)/(I_L + I_R)$, where $I_{L/R}$ is the luminescence intensity at the left-hand and right-hand ends of the nanopillar system, respectively. The experimental measurements display exactly the propagating trends observed in the predicted model of vortex excitation. A strong directionality of unpolarized luminescence can be achieved in our experiments for the high-order topological charges of $\ell = \pm 4$. To avoid any chiral information from light polarization, we used linearly polarized vortex beams to excite the nanopillar lattice. The experimental luminescence spectrum demonstrates a slightly large x-polarized component, which can be attributed to the strong transverse confinement in nanopillar array modes (Supplementary Figs. 13–15). These results confirm that the polarization information of the fundamental vortex beam is lost in the two-photon absorption process.

To further describe the experimental results, we analysed the orbit–orbit interaction in the nanopillar lattice. The directional PL emission is caused by the coupling of the excited vortex source into the one-dimensional nanopillar lattice. Distinguished from spin–orbit coupling, the electromagnetic waves, excited by vortex sources with topological charge $\ell = -4$, demonstrate identical directionality for $\sigma_\pm$ states, as shown in Fig. 3a. For unpolarized PL with equal $\sigma_\pm$ spin states, the total intensity distribution excited by the vortex source can

maintain directionality. To characterize the directionality, we simulated the time-average power flows toward the left-hand (P_L) and right-hand end (P_R) of the nanopillar lattice (Supplementary Note 3). Figure 3b shows the directionality D, defined as $D_{(x,y)} = (P_L - P_R)/(P_L + P_R)$, for the vortex source with $\ell = -4$ located at different positions. The sign of directionality D is flipped symmetrically on either side of the nanopillar lattice and shows a near-unity value close to the nanopillars. To characterize the coupling efficiency of the vortex source into the nanopillar lattice, we calculated the normalized position-dependent coupling strength $\zeta_{(x,y)} = (P_L + P_R)/(P_L + P_R)_{max}$, as shown in Fig. 3c. A hierarchical pattern is exhibited along the nanopillar lattice, which can be ascribed to the interference in periodic nanopillars. To describe the experimental phenomenon properly, the directional coupling efficiency, defined as $\kappa_{(x,y)} = D_{(x,y)} \times \zeta_{(x,y)}$, demonstrates the unidirectional coupling of the excited vortex source into the nanopillar lattice for controlling the PL emission (Fig. 3d). Note that the calculated directional coupling efficiency is dependent on the excited positions of the vortex source in our simulations.

For characterizing the incident vortex source, we calculated the OAM density on the transverse plane, as shown in Fig. 4a. To experimentally observe the position-dependent directionality, we changed the excited position by moving the vortex beam along the y axis. The experimental directionality D_{exp} of PL emission is demonstrated as a function of the excited positions, as shown in Fig. 4b. When the vortex beam is illuminated on the central area of the nanopillar system ($y = 0$), the D_{exp} is near zero. In our experiments, the directionality of PL emission was opposite when exciting the vortex beam on either side of the central axis (Supplementary Fig. 16). The unidirectional PL emission was consistent with the simulation results using a vortex electric multipole model. The maximum D_{exp} achieved in our experiments was smaller than the simulation results, which can be ascribed to the focal size of the excited vortex beam and the broadband PL spectrum. Considering the conservation law of the z-component of the total angular momentum j_z in the spatially symmetric nanostructures, we can theoretically calculate the directionality of luminescence by the coupling of vortex momentum density into the nanopillar lattice (see Supplementary Note 4 for details). The little deviation from theoretical predications is caused by the shape of the vortex source and the spatial symmetry of nanostructures. To confirm the orbit-directional coupling, we further studied the directional properties excited by vortex beams with different topological charges. Intriguingly, the directionality of PL emission can be changed by tuning the incident vortex beams (Fig. 4c). In particular, excited by the vortex beam with topological charge $\ell = +8$, we achieved a large directionality of $D_{exp} = 0.59$, which is markedly stronger than that by spin–orbit coupling (see Supplementary Fig. 17 and Supplementary Note 5 for details). The experimental data agree well with our theoretical results. As the spin information is lost in two-photon absorption processing, we cannot observe the spin–orbit coupling by unpolarized luminescence. For an intuitive comparison, we experimentally measured the directionality of $D_{exp} = 0.20$ excited by the vortex beam with topological charge $\ell = +1$, which has the same total intrinsic angular momentum j_z as the condition in spin–orbit coupling. In addition, the directionality of unpolarized luminescence could be further improved by using higher-order vortex sources for generating larger j_z states.

In summary, we have demonstrated that photonic OAM can control the directional emission of unpolarized luminescence in the one-dimensional nanopillar lattice at room temperature. The orbit-directional PL emission establishes a directional propagation in the nanopillar lattice, which may facilitate viable applications in on-chip optical communications and quantum information processing[35–37]. The directionality in the nanopillar lattice up to 0.59 has been experimentally recorded for the topological charge $\ell = +8$, which is substantially larger than that of the spin–orbit coupling and could be further increased by employing higher-order topological charges. The demonstrated directional propagation of the anti-Stokes shift PL with photonic OAM states could also be readily extended to other non-linear and luminescence processes[38]. Compared with circular dipoles, the vortex sources with higher-order intrinsic angular momenta can provide a platform for both fundamental studies and nanoscale optical applications in chiral quantum optics and the spin–orbit interaction of light[39]. Furthermore, the unidirectional propagation, without spin limitations, opens up unexplored and paradigm-shift opportunities for improving the directionality manipulation in other wave fields such as electron, sound and even molecular waves.

Online content

Any methods, additional references, Nature Portfolio reporting summaries, source data, extended data, supplementary information, acknowledgements, peer review information; details of author contributions and competing interests; and statements of data and code availability are available at https://doi.org/10.1038/s41566-023-01226-9.

References

1. Lodahl, P. et al. Chiral quantum optics. *Nature* **541**, 473–480 (2017).
2. Feng, L. et al. Experimental demonstration of a unidirectional reflectionless parity-time metamaterial at optical frequencies. *Nat. Mater.* **12**, 108–113 (2013).
3. Curto, A. G. et al. Unidirectional emission of a quantum dot coupled to a nanoantenna. *Science* **329**, 930–933 (2010).
4. Cihan, A. F., Curto, A. G., Raza, S., Kik, P. G. & Brongersma, M. L. Silicon Mie resonators for highly directional light emission from monolayer MoS2. *Nat. Photon.* **12**, 284–290 (2018).
5. Iyer, P. P. et al. Unidirectional luminescence from InGaN/GaN quantum-well metasurfaces. *Nat. Photon.* **14**, 543–548 (2020).
6. Rong, K. et al. Photonic Rashba effect from quantum emitters mediated by a Berry-phase defective photonic crystal. *Nat. Nanotechnol.* **15**, 927–933 (2020).
7. Bliokh, K. Y., Rodriguez-Fortuno, F. J., Nori, F. & Zayats, A. V. Spin–orbit interactions of light. *Nat. Photon.* **9**, 796–808 (2015).
8. Petersen, J., Volz, J. & Rauschenbeutel, A. Chiral nanophotonic waveguide interface based on spin-orbit interaction of light. *Science* **346**, 67–71 (2014).
9. Pan, D., Wei, H., Gao, L. & Xu, H. Strong spin-orbit interaction of light in plasmonic nanostructures and nanocircuits. *Phys. Rev. Lett.* **117**, 166803 (2016).
10. Rodríguez-Fortuño, F. J. et al. Near-field interference for the unidirectional excitation of electromagnetic guided modes. *Science* **340**, 328–330 (2013).
11. Barik, S. et al. A topological quantum optics interface. *Science* **359**, 666–668 (2018).
12. Guo, Q. et al. Routing a chiral Raman signal based on spin-orbit interaction of light. *Phys. Rev. Lett.* **123**, 183903 (2019).
13. Gong, S.-H., Alpeggiani, F., Sciacca, B., Garnett, E. C. & Kuipers, L. Nanoscale chiral valley-photon interface through optical spin-orbit coupling. *Science* **359**, 443–447 (2018).
14. Shreiner, R., Hao, K., Butcher, A. & High, A. A. Electrically controllable chirality in a nanophotonic interface with a two-dimensional semiconductor. *Nat. Photon.* **16**, 330–336 (2022).
15. Sun, L. et al. Separation of valley excitons in a MoS2 monolayer using a subwavelength asymmetric groove array. *Nat. Photon.* **13**, 180–184 (2019).
16. Liu, W. et al. Generation of helical topological exciton-polaritons. *Science* **370**, 600–604 (2020).
17. Deng, Y. et al. Circularly polarized luminescence from organic micro-/nano-structures. *Light: Sci. Appl.* **10**, 1–18 (2021).
18. Coles, R. et al. Chirality of nanophotonic waveguide with embedded quantum emitter for unidirectional spin transfer. *Nat. Commun.* **7**, 11183 (2016).

19. Uchida, M. & Tonomura, A. Generation of electron beams carrying orbital angular momentum. *Nature* **464**, 737–739 (2010).
20. Jiang, X., Li, Y., Liang, B., Cheng, J.-C. & Zhang, L. Convert acoustic resonances to orbital angular momentum. *Phys. Rev. Lett.* **117**, 034301 (2016).
21. Luski, A. et al. Vortex beams of atoms and molecules. *Science* **373**, 1105–1109 (2021).
22. Allen, L., Beijersbergen, M. W., Spreeuw, R. J. C. & Woerdman, J. P. Orbital angular-momentum of light and the transformation of Laguerre–Gaussian laser modes. *Phys. Rev. A* **45**, 8185–8189 (1992).
23. Ni, J. et al. Gigantic vortical differential scattering as a monochromatic probe for multiscale chiral structures. *Proc. Natl Acad. Sci. USA* **118**, e2020055118 (2021).
24. Ji, Z. et al. Photocurrent detection of the orbital angular momentum of light. *Science* **368**, 763–767 (2020).
25. Yao, A. M. & Padgett, M. J. Orbital angular momentum: origins, behavior and applications. *Adv. Opt. Photon.* **3**, 161–204 (2011).
26. Ouyang, X. et al. Synthetic helical dichroism for six-dimensional optical orbital angular momentum multiplexing. *Nat. Photon.* **15**, 901–907 (2021).
27. Miao, P. et al. Orbital angular momentum microlaser. *Science* **353**, 464–467 (2016).
28. Zhang, Z. et al. Tunable topological charge vortex microlaser. *Science* **368**, 760–763 (2020).
29. Ren, H. et al. Orbital-angular-momentum-controlled hybrid nanowire circuit. *Nano Lett.* **21**, 6220–6227 (2021).
30. Bliokh, K. Y. Geometrical optics of beams with vortices: Berry phase and orbital angular momentum Hall effect. *Phys. Rev. Lett.* **97**, 043901 (2006).
31. Garbin, V. et al. Mie scattering distinguishes the topological charge of an optical vortex: a homage to Gustav Mie. *New J. Phys.* **11**, 013046 (2009).
32. Devlin, R. C., Ambrosio, A., Rubin, N. A., Mueller, J. B. & Capasso, F. Arbitrary spin-to-orbital angular momentum conversion of light. *Science* **358**, 896–901 (2017).
33. Inoue, T. & Hori, H. Theoretical treatment of electric and magnetic multipole radiation near a planar dielectric surface based on angular spectrum representation of vector field. *Opt. Rev.* **5**, 295–302 (1998).
34. McArthur, D., Yao, A. M. & Papoff, F. Scattering of light with angular momentum from an array of particles. *Phys. Rev. Research* **2**, 013100 (2020).
35. Ni, J. et al. Multidimensional phase singularities in nanophotonics. *Science* **374**, eabj0039 (2021).
36. Qiao, X. et al. Higher-dimensional supersymmetric microlaser arrays. *Science* **372**, 403–408 (2021).
37. Ren, H., Li, X., Zhang, Q. & Gu, M. On-chip noninterference angular momentum multiplexing of broadband light. *Science* **352**, 805–809 (2016).
38. Kruk, S. et al. Nonlinear light generation in topological nanostructures. *Nat. Nanotechnol.* **14**, 126–130 (2019).
39. Jin, Z. et al. Phyllotaxis-inspired nanosieves with multiplexed orbital angular momentum. *eLight* **1**, 5 (2021).

Publisher's note Springer Nature remains neutral with regard to jurisdictional claims in published maps and institutional affiliations.

Springer Nature or its licensor (e.g. a society or other partner) holds exclusive rights to this article under a publishing agreement with the author(s) or other rightsholder(s); author self-archiving of the accepted manuscript version of this article is solely governed by the terms of such publishing agreement and applicable law.

© The Author(s), under exclusive licence to Springer Nature Limited 2023

Methods

Sample fabrication and characterization

The one-dimensional nanopillar lattice used in our experiments was fabricated by direct laser writing in a commercially available zirconium–silicon hybrid sol–gel material doped with 4,4′-bis(diethylamino)-benzophenone photoinitiator (SZ2080, IESL-FORTH). We added rhodamine 6 G molecules (Sigma-Aldrich) with the concentration of 20 mg ml^{-1} in the polymer material as a photosensitizer for generating anti-Stokes shift luminescence at the visible regime. Before laser polymerization, the pre-baking process was set 30 min on a 100 °C thermal platform to evaporate the solvent of polymer material. After engineering the nanopillar lattice, the photopolymerized material was developed in 1-propanol until all the unpolymerized part was washed away. The SEM image was taken by a secondary electron SEM (ZEISS EVO18) with an accelerating voltage of 10 keV after depositing ~10 nm gold on the sample.

Experimental setup for PL measurements

A mode-locked Ti:sapphire ultrafast oscillator (Chameleon Vision-S, Coherent Inc.) was used as the femtosecond laser source. The central wavelength of the laser is 800 nm, with a pulse width of 75 fs and a repetition rate of 80 MHz. The phase-only reflective liquid-crystal spatial light modulator (Pluto NIR-2, Holoeye Photonics AG) has 1,920 × 1,080 pixels, with a pixel pitch of 8 μm, on which computer-generated holograms with different topological charges can be displayed. A general ×100 dry objective lens (NA = 0.9, Olympus) was used to focus the generated vortex beams in the nanopillar sample. The sample was mounted on a 3D-piezo-nanostage (E545, Physik Instrumente) with nanoscale resolution to precisely tune the locations of nanostructures under optical microscopy. The PL intensity distribution was caught by a charge-coupled device camera (MindVision HD-SUA133GM-T camera, image area: 1,280 × 1,024 pixels) with the acquisition time of 30 ms. The pump power of the incident vortex beams was tunable for achieving clarified PL optical images on the charge-coupled device camera.

Numerical simulation of excitation with circularly polarized dipoles

The electromagnetic simulations were performed using a commercial full-wave finite-difference time-domain software (Lumerical FDTD Solutions, Inc.). One x-polarized electric dipole and one y-polarized electric dipole, out-of-phase by 90°, were selected as a circular dipole. To simulate the vortex sources, we used multiple circular dipoles with phase gradient in a circular distribution. Twelve circularly polarized dipoles accompanied by a gradient phase of $2\pi\ell$ were selected as the excited vortex source with topological charge $\ell = \pm 4$. The structural parameters of the nanopillar lattice in our simulations are consistent with the actual dimensions, which were extracted from the SEM images. The centre of the vortex source was located at $y = 200$ nm with respect to the nanopillar system. In the simulation, the refractive index of the dielectric nanopillar was set to be 1.5 and the operating wavelength was set at 560 nm. Perfectly matched layer boundaries were employed for the x and y directions in the two-dimensional simulations. The location of the vortex source was swept for simulating the position-dependent directionality.

Data availability

The data that support the findings of this study are available from the corresponding authors upon reasonable request.

Acknowledgements

This work was supported by the National Natural Science Foundation of China (Grant Nos. 61927814, 52122511, 52075516, 61805230, 62105319 and U20A20290; W.D., J.L., S.J. and Y.H.), the USTC Research Funds of the Double First-Class Initiative (Grant No. YD2090002005; W.D.), the National Key R&D Program of China (Grant No. 2021YFF0502700; W.D.) and the Foundation of Equipment Development Department (Grant No. 6140922010901; W.D.). J.N. acknowledges support from the start-up funding of the University of Science and Technology of China and the CAS Talents Program. We thank the USTC Center for Micro and Nanoscale Research and Fabrication. C.W.Q. is supported by the National Research Foundation, Prime Minister's Office, Singapore under Competitive Research Program Award NRF-CRP22-2019-0006.

Author contributions

J.N. and C.W.Q. conceived the idea and developed the theory. S.J., S.L. and Z.W. performed the experiments. J.N. performed the simulations. J.N., Y.C., X.L. and S.J. analysed the data. J.N., C.W.Q. and D.W. wrote the manuscript. C.W.Q. and D.W. supervised the project. All authors discussed the results and commented on the manuscript.

Competing interests

The authors declare no competing interests.

Additional information

Supplementary information The online version contains supplementary material available at https://doi.org/10.1038/s41566-023-01226-9.

Correspondence and requests for materials should be addressed to Dong Wu or Cheng-Wei Qiu.

Peer review information *Nature Photonics* thanks the anonymous reviewers for their contribution to the peer review of this work.

Reprints and permissions information is available at www.nature.com/reprints.